KEK Isotope Separation System (KISS)

KEK RNB group (e-mail contact address : KISS_contact@kek.jp)
Institute of Particle and Nuclear Studies (IPNS),
High Energy Accelerator Research Organization (KEK), Ibaraki 305-0801, Japan

March 20, 2015

1 Introduction

KISS is a mass-separator of radioactive isotopes ionized by laser resonance ionization method. This device has been developed to perform our research project relevant to the nuclear astrophysics [1]. In this project, we will study lifetimes of neutron-rich unknown nuclei, at first, in the region around $A \sim 195$ and $N = 126$, where is very close to the expected waiting nuclei for the third abundance peak of rapid neutron capture process. Unknown nuclei will be produced in the multi-nucleon transfer reactions of ^{136}Xe and ^{198}Pt.

KISS has a characteristic capability to separate a single isotope specified by its mass number (A) and the atomic number (Z) from huge amount of other isotopes produced in the reaction. Apart from our research project, the separator KISS can be suitable tool for scientific researches on the ground state properties in neutron-rich heavy nuclides. In this note we will provide some expertise obtained in the KISS development to promote any experimental ideas of you. Our project welcomes the participation of all of you, who is considering to study this kind of subject under the collaboration with us.

2 Multi-nucleon transfer reaction of ^{136}Xe and ^{198}Pt system

The MNT reaction between two heavy ions at the low energy around the Coulomb barrier is considered as a promising tool to produce and investigate neutron-rich nuclei. The reactions have been studied intensely. However, the mechanism of the reaction is not fully understood. The GRAZING [2, 3] calculation, which is often used for comparison with MNT measurements, does not reproduce the experimental data in terms of absolute cross sections and mass distributions in massive transfer channels. In order to investigate the effectiveness of the reaction system of ^{136}Xe+^{198}Pt, we have studied reaction products of the system by using the large acceptance magnetic spectrometer VAMOS++ and the high efficiency gamma detector array EXOGAM at GANIL [4].

Figure 1 shows the distribution of the projectile-like fragments (PLFs) detected by the VAMOS++. The abscissa indicates the mass and the ordinate indicates the atomic number. The obtained resolutions of mass and atomic numbers are M/ΔM$\sim$200, Z/ΔZ$\sim$60, respectively. The color code indicates the detected number of events. It shows the sizable contributions of the proton

pick-up and neutron stripping channels compared with the ones of the proton stripping and neutron pick-up channels. Considering particle evaporation from the primary fragments, we could expect production cross sections for the TLFs of our interest as much as those predicted by GRAZING code at the region in $N \sim 126$ and larger cross sections by orders of magnitude at the peak of the isotopic distributions. The expected production rate by the reaction between ^{136}Xe beam (8.12 MeV/nucleon, 10 pnA) and ^{198}Pt target (6 mg/cm^2) are listed (see the appendix).

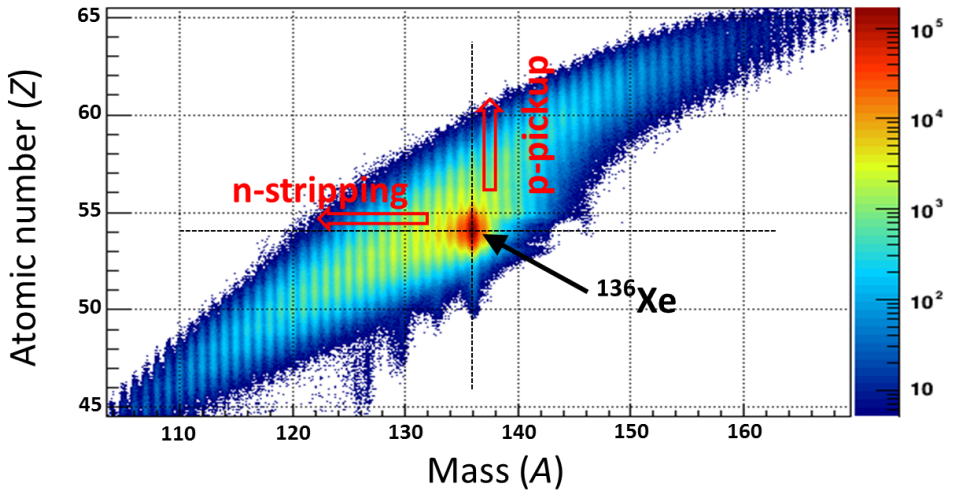

Figure 1: Isotope distribution of the PLFs detected by the VAMOS++.

3 Outline of the present KISS

Figure 2 shows a schematic layout of KISS, which was constructed at the RIBF facility in RIKEN at the beginning of 2011. It consists of a laser system, a mass-separator system, the decay measurement stations and a gas-cell system.

The laser system consists of two frequency-tunable dye lasers pumped by two excimer (XeCl, 308 nm) lasers and was installed in a separate room below the KISS gas cell system. A repetition rate of up to 200 Hz is used for saturation of an ionization efficiency in the gas cell, and the bandwidth of the dye laser is 0.15 cm^{-1}. The frequency of the first step laser is doubled using a second harmonic generator (BBO crystal). The distance between the laser system and the gas cell is about 15 m. In the gas cell, both lasers overlap for resonance ionization, spatially and temporally.

The ion-optical configuration is EQD-MD-MQD-Focal point 1 (F1)-EQT-Focal point 2 (F2)-Detection point, where EQD, MD, MQD and EQT are electrostatic quadrupole doublet, magnetic dipole, magnetic quadrupole doublet and electrostatic quadrupole triplet, respectively. F1 indicates the first focal point, where a slit system (R/L and U/D along the beam direction) is available. The basic parameters of the ion-optical elements are listed in Table 1. Mass dispersion, measured mass

resolving power and the beam spot size at F1 are 2.06 cm/%, 900 and 2 mm in FWHM, respectively. Beam intensity monitors were set at F1, F2, and the detection point. A two-dimensional MCP beam profile monitor was installed at the F2 [5].

Table 1: Basic parameters of KISS ion-optical elements

Element	Geometry
EQ	$r_{\mathrm{bore}} = 30$ mm, $L = 100$ mm
MD	$\rho_{\mathrm{D}} = 1353$ mm, $\theta_{\mathrm{D}} = 45°$, Gap= 70 mm
MQ	$r_{\mathrm{bore}} = 65$ mm, $L = 100$ mm

Decay measurement station has a tape transport device for avoiding the radioactivities in the decay chain of separated nuclides under pulsed beam operation of the KISS. There is one tape transport device at this moment. In the near future, three devices will be constructed as shown in Fig. 2. Two layered plastic scintillator telescopes for β-rays followed by three Clover-type germanium detectors for γ-rays cover the implantation point in the tape transport device. Typical beam size of this point is collimated with a diameter of 8mm. The telescopes cover around 90% of 4π, and the efficiency of three germanium detectors are 15% for γ-ray with the energy of 500 keV. The background rate of the present β-ray telescopes is 0.7 cps. In order to measure the lifetime of nuclei with $N = 126$ whose production rate are around a few cps, we will install a newly designed β-ray telescopes, in 2015, whose background rate is expected to be reduced down to 0.1 cps. For further lifetime measurements under the lower production rate, we have started to develop a low-background β-ray counter (gas counter) in order to suppress the background rate to the level of several cph. The gas counter system will be installed at the beginning of 2016.

3.1 Gas cell system dedicated for the MNT reactions of ^{136}Xe and ^{198}Pt

The gas-cell system includes an argon gas feeding line with a gas-purification device (Monotorr Phase II 3000), a gas-catcher cell, and a sextupole ion-guide (SPIG) [6] (See Fig. 3). To enable extraction of isotopes as an ion beam with sufficiently low emittance and high efficiency, the gas-cell system employs differential pumping system which makes different stages of vacuum in the vacuum chamber from 50 kPa to several 10^{-4} Pa. The vacuum chamber of the gas-cell system is separated into three rooms for the differential pumping. The first, second and third rooms are pumped down by a 175 l/s screw pump, two 800 l/s turbo molecular pumps (TMPs) and a 1500 l/s TMP, respectively. The three neighboring rooms are connected by the SPIG with an aperture of 3 mm diameter and 200 mm length. The gas cell filled with argon gas at a pressure of 50 kPa is placed in the first room. The second room is important for differential pumping and ensures that the vacuum conditions in the third room are sufficient for applying a high voltage to the first and second rooms (several 10^{-4} Pa). Typical pressure values in the three rooms are $P_1 = 8.7$ Pa, $P_2 = 0.9$ Pa and $P_3 = 3{\times}10^{-4}$ Pa, for $P_{\mathrm{G}} = 50$ kPa [7]. The present differential pumping system enables to operate the gas cell (exit diameter of 1mm) up to $P_{\mathrm{G}} = 88$ kPa, which is limited by the conductance of the pressure control valve.

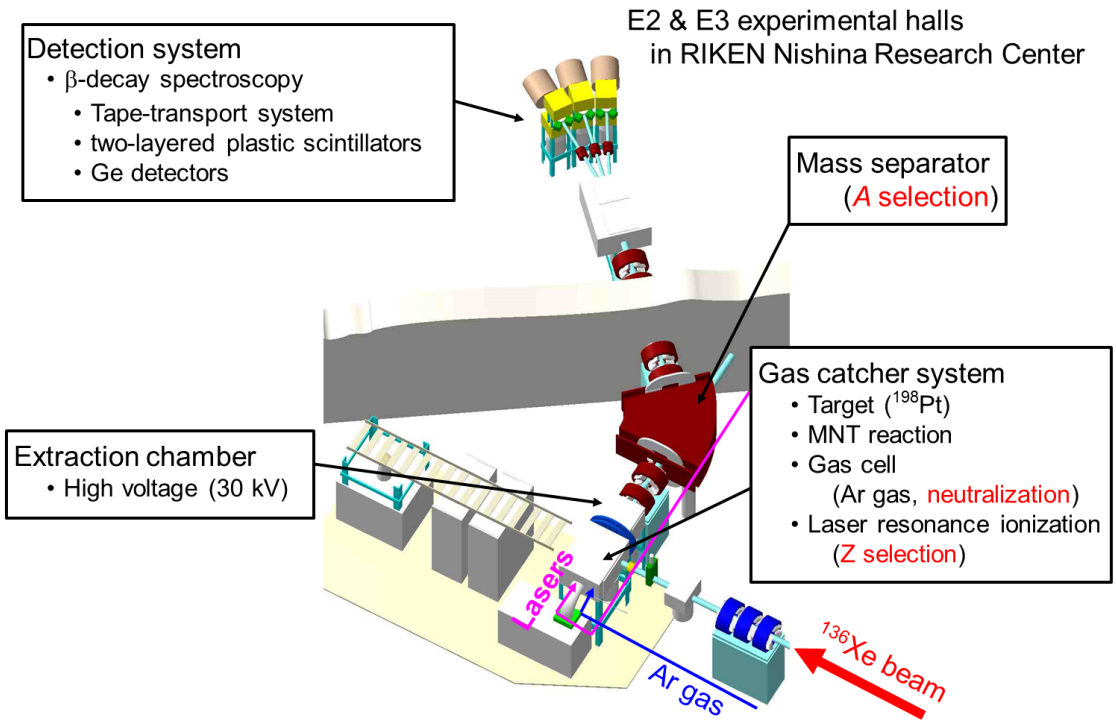

Figure 2: Schematic layout of KISS.

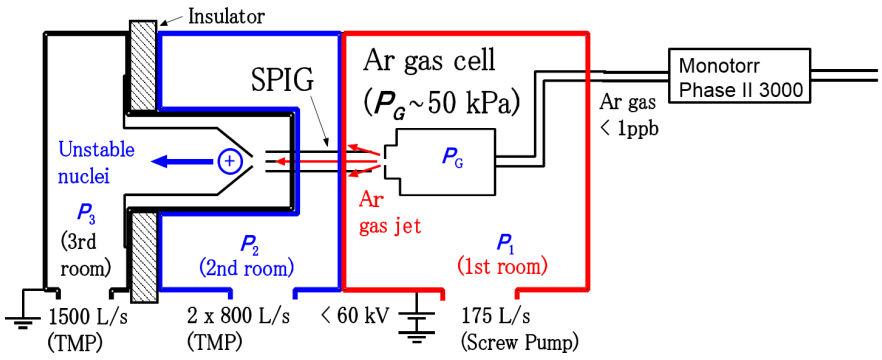

Figure 3: Schematic view of the gas-cell system. The boundaries of the first, second and third rooms are indicated by the thick red, blue and black lines, respectively.

Figure 4-(a) shows the calculated stopping distribution of ^{202}Os in argon gas with a pressure of 50 kPa. The energies and emission angles of the ^{202}Os nuclei were calculated by the GRAZING code [2, 3] and the stopping power was calculated by the SRIM2008 code [8]. The stopping distribution exhibits a wide spread. Therefore, a large gas cell volume ($\sim$ 480 cm^3) was considered to obtain a high efficiency (90%), as shown in Fig. 4-(b).

Considering the stopping distribution of ^{202}Os and the macroscopic motion due to gas flow (flow velocity) and diffusion, transport efficiency is calculated to be 40% by Monte Carlo method, where the rest is lost at the wall due to diffusion. In the simulation, the position and velocity of an atom in the gas cell were calculated by means of a fixed time-step ray-tracing algorithm until collision with the gas cell wall or transport to the exit. Figure 5 shows the calculated argon gas flow trajectories based on the exact geometry in Fig. 4-(b). The pressure of the argon gas is 50 kPa, and the color code indicates the flow velocity (m/s). The extraction efficiency is estimated to be about 5% for ^{200}W ($Z = 74$, $N = 126$) nuclei with a half-life time of 423 ms predicted by the KUTY model [9]. ^{200}W nuclei is located most far from the stability line in the project.

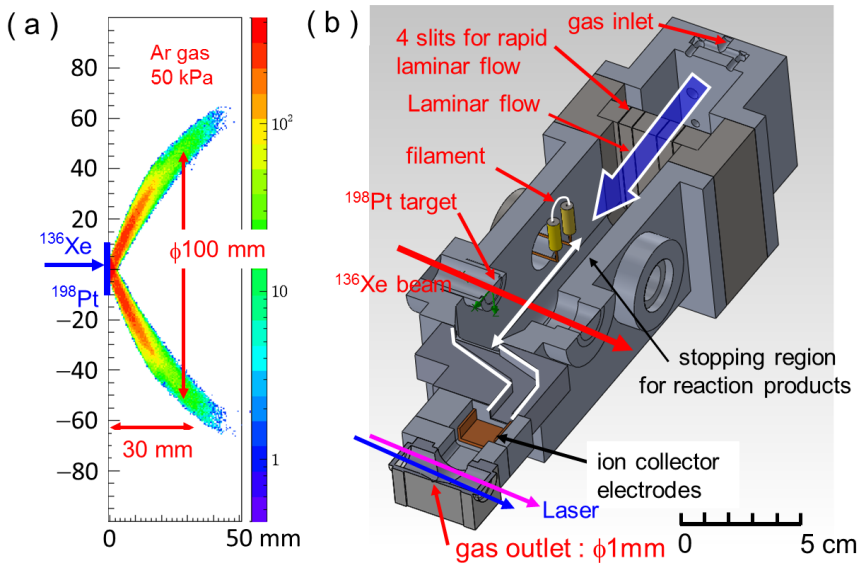

Figure 4: (a) Stopping distribution of ^{202}Os in argon gas with a pressure of 50 kPa. (b) Schematic cross sectional view of the gas cell.

4 Present performance

Figure 6 shows the measured extraction time profile of ^{56}Fe from the stopping region by using iron filament at off-line test. The time profile was in good agreement with the simulated one. This result allows to expect that the laminar flow for quick and efficient transport would be generated as the simulation. In the case of the stable ^{193}Ir generated by the filament, the mean-extraction time was 300 ms which was slower than ^{56}Fe case. However, this value is shorter than the expected lifetime ($t_{1/2} = 423$ ms) for ^{200}W.

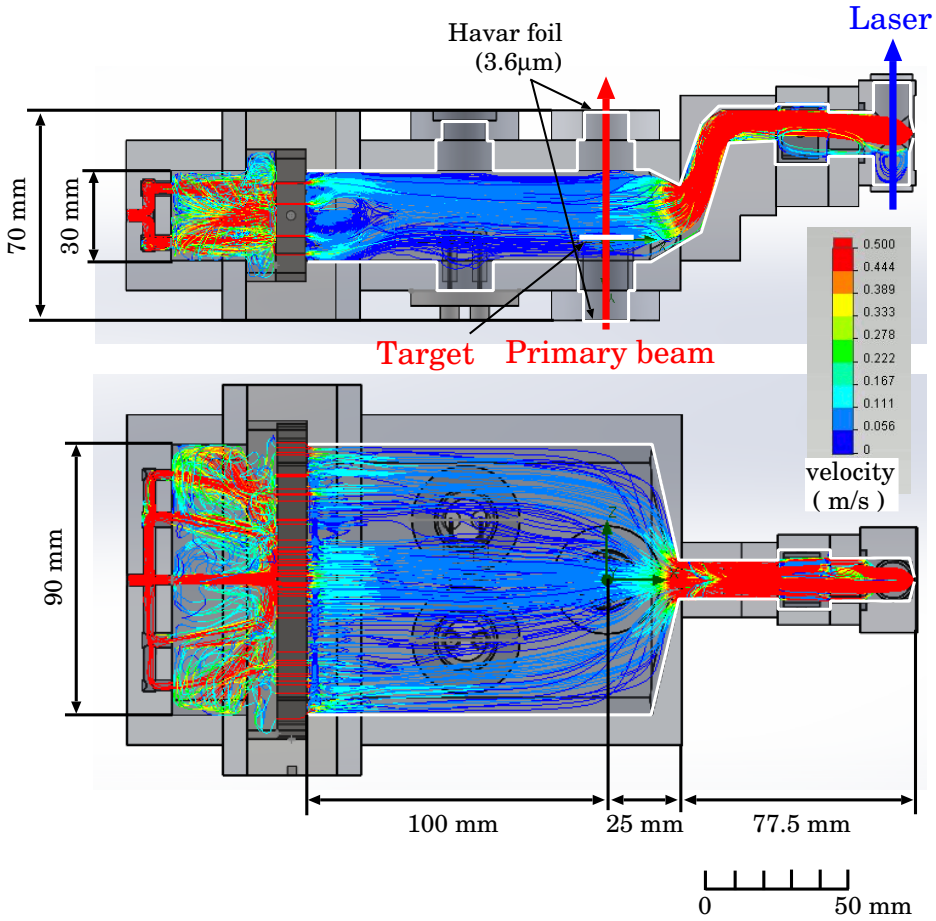

Figure 5: Calculated argon-gas flow-trajectories. (a) top view and (b) face view of the gas cell. The boundary of the gas-cell main part is indicated by white lines.

4.1 On-line test

The absolute extraction efficiency and beam purity of KISS were evaluated by on-line tests. In the case of ^{56}Fe beam, the efficiency was evaluated by measuring the beam intensities implanted in and extracted from the gas cell. In the case of ^{198}Pt beam, the efficiency was evaluated from the ratio of the calculated stopping yield of elastic events of ^{198}Pt to the measured intensities extracted from the gas cell.

4.1.1 Extraction ^{56}Fe

We measured the extraction efficiency and purity as shown in Figs. 7. The efficiency was about 0.25%, and was independent from the primary beam intensity as shown in Fig. 7-(a) owing to the bend structure of the gas cell. In Fig. 7-(b), the purity was more than 98% and slightly depended on the primary beam intensity. The beam purity decreased with increasing the primary beam intensity. However, more than 90% of purity is enough pure to measure the lifetime of nuclei with

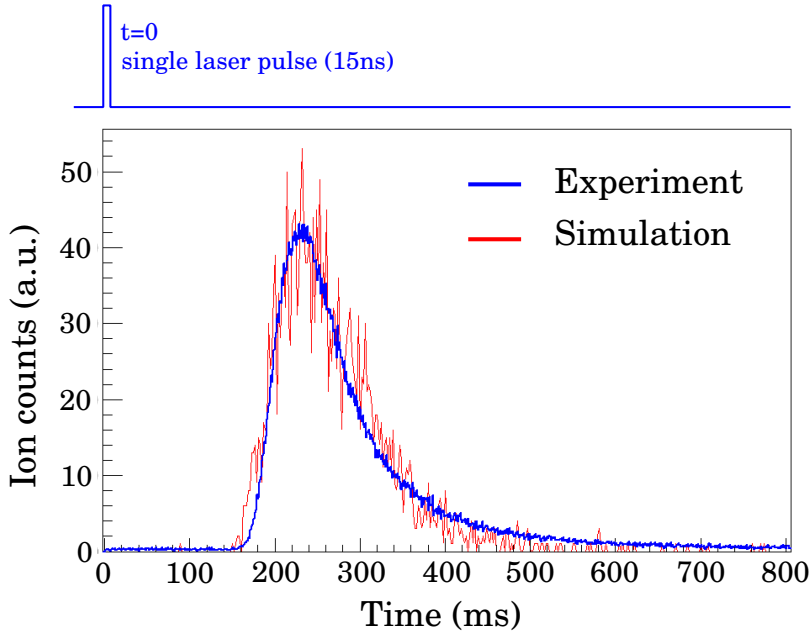

Figure 6: Time profile of ^{56}Fe evaporated from the filament and ionized at the primary beam position. The blue and red lines indicate the experimental and simulated results, respectively.

$N = 126$ in the present project.

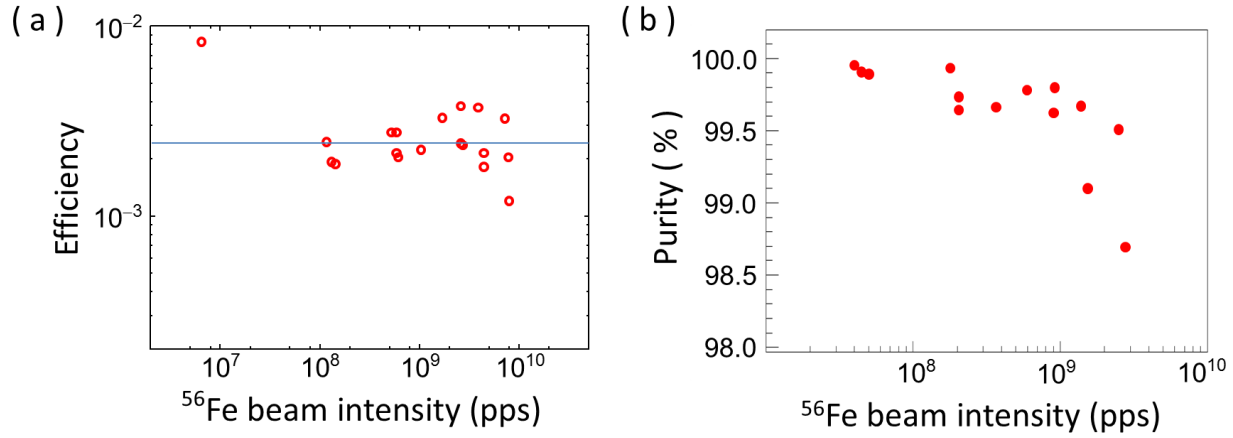

Figure 7: (a) Extraction efficiency of ^{56}Fe ions and (b) beam purity measured as a function of ^{56}Fe beam intensity.

4.1.2 Extraction ^{198}Pt and ^{199}Pt

On-line tests using the ^{136}Xe beam was performed with the energy of 10.75 MeV/nucleon and the maximum intensity of 20 pnA. The ^{136}Xe beam was directed on to the ^{198}Pt target placed in the gas cell, and was stopped at a tungsten beam dumper after passing through the gas cell. The thermalized and neutralized ^{198,199}Pt atoms of the reaction products were re-ionized in the gas cell. The ions were extracted and detected after mass separation by using the Channeltron detector for ion counting. The lifetime of ^{199}Pt was measured by using the β-ray telescopes installed at the decay measurement station.

We extracted laser-ionized ^{198}Pt atoms emitted from the target by elastic scattering. However, the ^{198}Pt ions formed molecular ions such as $^{198}PtH_2^+$, $^{198}PtH_2O^+$, and $^{198}PtAr_2^+$ with the intensity ratio of 1, 1, and 6 relative to the intensity of $^{198}Pt^+$ ions. Figure 8 shows the measured extraction efficiency of the $^{198}PtAr_2^+$ molecular ions ($A = 278$) as a function of the primary beam intensity. The extraction efficiency was defined as the ratio of the number of $^{198}PtAr_2^+$ ions detected to the number of ^{198}Pt atoms emitted from the target by elastic scattering (17 barn), respectively. The efficiency of about 0.20% was observed to be independent of the primary beam intensity, as shown in Fig. 8. The separated beam purity was $> 99.7\%$ at the maximum primary beam intensity of 20 pnA.

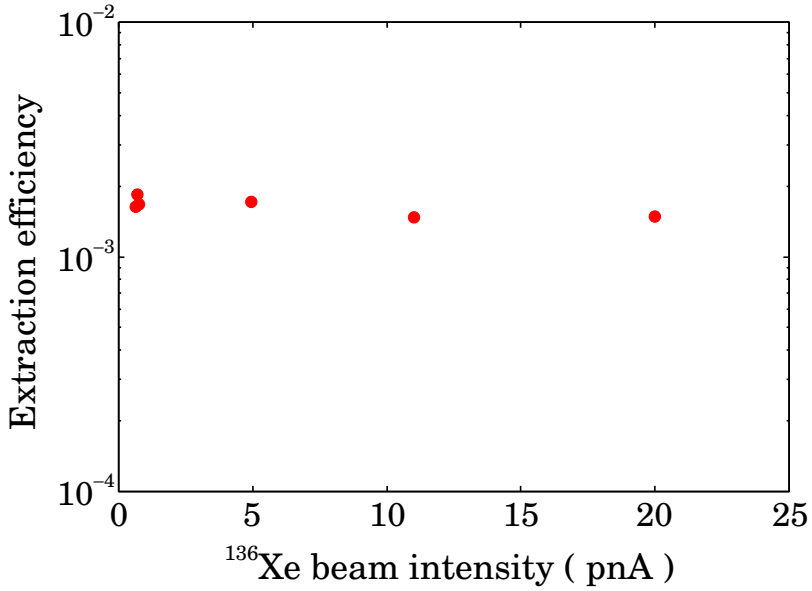

Figure 8: Extraction efficiency of $^{198}PtAr_2^+$ molecular ions measured as a function of ^{136}Xe beam intensity.

We also extracted laser-ionized ^{199}Pt ($t_{1/2} = 30.8(2)$ min.) atoms which mainly formed $^{199}PtAr_2^+$ molecular ions like ^{198}Pt. Figure 9 shows the measured lifetime by using $^{199}PtAr_2^+$ molecular ions. The measured lifetime of $t_{1/2} = 33(4)$ min. was in good agreement with the reported value. Thus, the molecular formation does not affect the lifetime measurement of unstable nuclei.

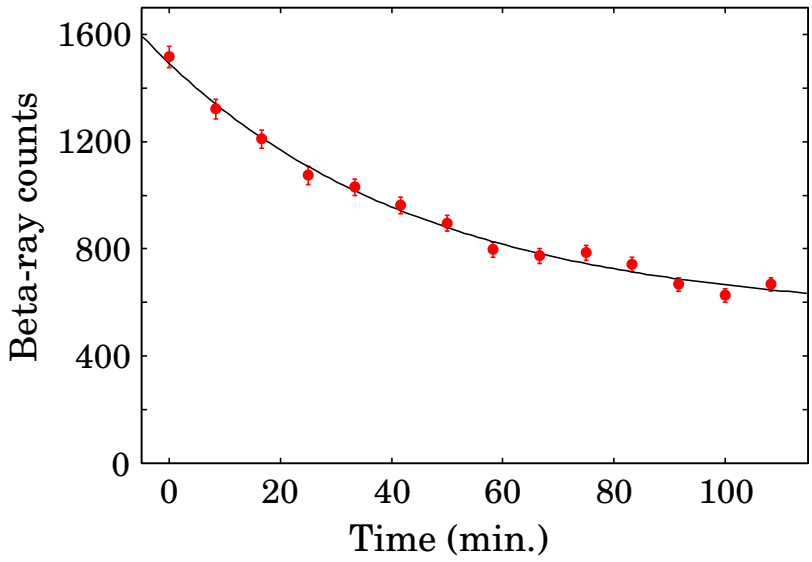

Figure 9: Lifetime measurement of ^{199}Pt.

5 Accessible region on nuclear chart

From the measured extraction efficiency of 0.25% and 0.20% for $^{56}Fe^{+}$ and $^{198}PtAr_2^{+}$ cases, we expect that the extraction efficiency would be more than 0.1% for the heavy elements of nuclei around $N = 126$. Figure 10 shows an accessible region for lifetime measurement of nuclei around $N = 126$ on nuclear chart. The yellow line indicates a boundary for the region of measured half lifetime. Even with the efficiency of 0.1%, it is feasible to measure the lifetime of more than 12 nuclei newly and access up to ^{202}Os by using the MNT reaction of ^{136}Xe beam with the intensity of 10 pnA. By increasing the efficiency, we can extend the accessible region. At the first stage of KISS project, we plan to reach up to ^{200}W and measure the half-lives with an efficiency of 1%.

In order to estimate how far we can access and measure the lifetime of nuclei with $N = 126$, we plan to measure the efficiency of each heavy elements of our interest by using ^{136}Xe beam and ^{198}Pt (^{187}Re) target system. For this purpose, platinum ($Z = 78$) and rhenium ($Z = 75$) production targets will be used to produce elastic particles of ^{198}Pt and ^{187}Re, and MNT reaction products of ^{201}Pt, ^{196}Ir and ^{195}Os emitted from ^{198}Pt target, and ^{191}Re, ^{189}W and ^{187}Ta emitted from ^{187}Re target as well. The MNT reaction products of heavy elements are close to the targets and are produced with larger production cross sections in order to promote the efficient developments.

6 Other region on nuclear chart

It is possible to access other region on nuclear chart by changing the combination of the primary beam and the production target. According to the kinematics of a reaction system, the kinetic energy of the reaction product of interest will change. It would be necessary to modify the geometry

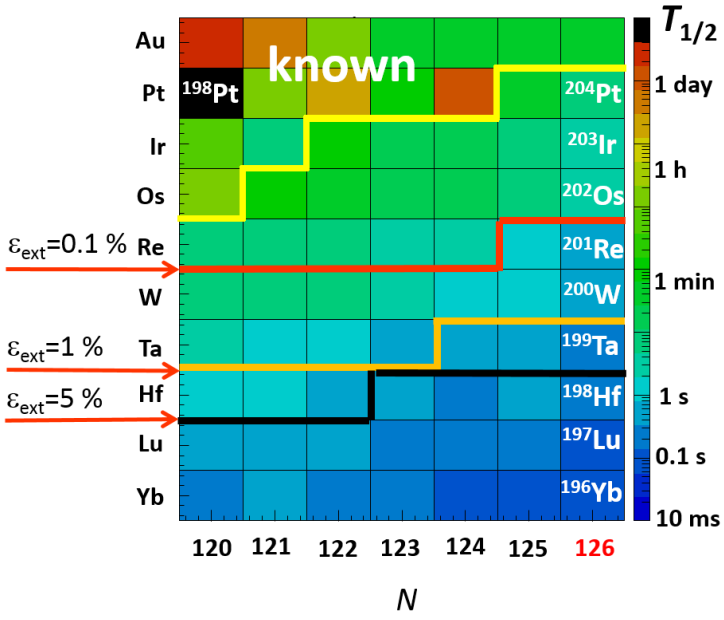

Figure 10: Accessible region for lifetime measurement on nuclear chart using the ^{136}Xe beam with the intensity of 10 pnA for different extraction efficiency. The color codes indicate the calculated half lifetime by the KUTY model [9].

of the gas cell and search for an ionization scheme. In that sense, we would like to discuss for feasibility of each subjects presented in the LOIs, which is expected to give other reaction systems different from the one of ^{136}Xe and ^{198}Pt.

Appendix

Table 2 shows production rates of unstable nuclei by the reaction between ^{136}Xe beam (8.12 MeV/nucleon, 10 pnA) and ^{198}Pt target (6 mg/cm^2) expected from calculations by the GRAZING code [10]. $T_{1/2}$ indicates half-life from WWW chart of the nuclides 2010 at nuclear data center, JAEA tokai [11]. The values in parentheses indicate estimated half-life values. Note that it is necessary to take into account the KISS overall efficiency of 0.15% at this moment and the survival efficiency against the β-decay losses. The survival efficiency can be estimated by considering the extraction time of 370 ms from the gas cell.

Table 2: Production rates estimated by the GRAZING code.

Nuclide	$T_{1/2}$	Yield (pps)	Nuclide	$T_{1/2}$	Yield (pps)	Nuclide	$T_{1/2}$	Yield (pps)
^{196}Tl	1.8 h	1.7×10^2	^{205}Au	31 s	1.2×10^2	^{198}Os	(2.8 m)	4.0×10^2
^{197}Tl	2.8 h	5.7×10^2	^{206}Au	(1.5 s)	18	^{199}Os	(35 s)	1.5×10^2
^{198}Tl	5.3 h	1.1×10^3	^{191}Pt	2.8 d	2.6×10^2	^{200}Os	(38 s)	84
^{199}Tl	7.4 h	1.8×10^3	^{193}Pt	50 y	3.9×10^3	^{201}Os	(11 s)	22
^{200}Tl	1.1 d	1.7×10^3	^{197}Pt	20 h	1.3×10^5	^{202}Os	(6.3 s)	6.7
^{201}Tl	3.0 d	1.7×10^3	^{199}Pt	31 m	1.6×10^5	^{203}Os	(333 ms)	1.3
^{202}Tl	12 d	1.0×10^3	^{200}Pt	13 h	4.7×10^4	^{188}Re	17 h	5.9
^{204}Tl	3.8 y	2.1×10^2	^{201}Pt	2.5 m	9.2×10^3	^{189}Re	1.0 d	9.3
^{206}Tl	4.2 m	17	^{202}Pt	1.8 d	2.5×10^3	^{190}Re	3.1 m	12
^{207}Tl	4.8 m	5.1	^{203}Pt	(3.0 m)	6.1×10^2	^{191}Re	9.8 m	20
^{208}Tl	3.1 m	1.0	^{204}Pt	(1.6 m)	1.7×10^2	^{192}Re	16 s	32
^{193}Hg	3.8 h	1.2×10^2	^{205}Pt	(1.4 s)	22	^{193}Re	(1.6 m)	46
^{194}Hg	444 y	3.3×10^2	^{194}Ir	19 h	3.4×10^3	^{194}Re	(15 s)	38
^{195}Hg	11 h	8.1×10^2	^{195}Ir	2.5 h	6.8×10^3	^{195}Re	(20 s)	43
^{197}Hg	2.7 d	3.4×10^3	^{196}Ir	52 s	9.6×10^3	^{196}Re	(5.5 s)	29
^{203}Hg	47 d	7.0×10^2	^{197}Ir	5.8 m	2.0×10^4	^{197}Re	(11 s)	25
^{205}Hg	5.1 m	92	^{198}Ir	8 s	9.0×10^3	^{198}Re	(3.8 s)	9.2
^{206}Hg	8.3 m	30	^{199}Ir	(3.6 m)	4.4×10^3	^{199}Re	(3.7 s)	5.4
^{207}Hg	2.9 m	4.6	^{200}Ir	(25 s)	1.5×10^3	^{200}Re	(1.4 s)	1.8
^{195}Au	186 d	5.7×10^3	^{201}Ir	(45 s)	6.5×10^2	^{188}W	70 d	1.4
^{196}Au	6.2 d	9.5×10^3	^{202}Ir	(9.9 s)	2.0×10^2	^{189}W	11 m	1.4
^{198}Au	2.7 d	2.3×10^4	^{203}Ir	(8.7 s)	66	^{190}W	30 m	2.2
^{199}Au	3.1 d	4.9×10^4	^{204}Ir	(435 ms)	9.8	^{191}W	(1.6 m)	2.1
^{200}Au	48 m	2.6×10^4	^{193}Os	1.3 d	5.2×10^2	^{192}W	(1.0 m)	2.6
^{201}Au	26 m	9.9×10^3	^{194}Os	6.0 y	8.6×10^2	^{193}W	(16 s)	2.0
^{202}Au	28 s	3.4×10^3	^{195}Os	6.5 m	7.5×10^2	^{194}W	(13 s)	2.8
^{203}Au	1.0 m	1.5×10^3	^{196}Os	35 m	1.0×10^3	^{195}W	(5.9 s)	1.6
^{204}Au	40 s	3.5×10^2	^{197}Os	(1.3 m)	5.2×10^2	^{196}W	(8.0 s)	1.2

References

[1] S. C. Jeong *et al.*, *KEK Report* 2010-2 (2010) and references listed in http://kekrnb.kek.jp/en/publications.html.

[2] A. Winther, *Nucl. Phys. A* **572** 191–235 (1994).

[3] A. Winther, *Nucl. Phys. A* **594** 203–245 (1995).

[4] Y. X. Watanabe *et al.*, *Nucl. Instr. and Meth. B* **317** 752–755 (2013).

[5] H. Ishiyama *et al.*, *RIKEN Accele. Prog. Rep.* **45**, 151 (2012).

[6] H.J. Xu *et al.*, *Nucl. Instru. and Meth. A* **333** 274–281 (1993).

[7] Y. Hirayama *et al.*, *RIKEN Accele. Prog. Rep.* **45** 152 (2012).

[8] J. F. Ziegler, http://www.srim.org/.

[9] T. Tachibana and M. Yamada, *Proc. Inc. Conf. on exotic nuclei and atomic masses*, Arles, 763 (1995).

[10] http://personalpages.to.infn.it/ nanni/grazing/

[11] http://wwwndc.jaea.go.jp/CN10/index.html